Chemical transfer during redox exchanges between H-2 and Fe-bearing silicate melts.

Fabrice Gaillard, Michel Pichavant, Stephen Macwell, Rémi Champallier, Bruno Scaillet, Catherine Mccammon

American Mineralogist, Volume 88, pages 308–315, 2003

Chemical transfer during redox exchanges between H_2 and Fe-bearing silicate melts

FABRICE GAILLARD,[1,*] MICHEL PICHAVANT,[1] STEPHEN MACKWELL,[2] RÉMI CHAMPALLIER,[1] BRUNO SCAILLET,[1] AND CATHERINE MCCAMMON[2]

[1]CNRS, ISTO- 1 A rue de la Férollerie, Orléans cedex 02 45071, France
[2]Bayerisches Geoinstitut, Universität Bayreuth, D-95440 Bayreuth, Germany

ABSTRACT

Kinetics and reaction paths of Fe^{3+} reduction by H_2 in high-Fe and low-H_2O silicate melts have been investigated at 800 °C. Time-series experiments were performed in cold-seal pressure vessels at 50 bars of pure H_2 using rapid-heating and rapid-quench strategies. Within the first minutes of the experiments, a fast partitioning of Na occurred between the gas and the melt due to the reducing conditions. Kinetically decoupled from the Na partitioning, the progression of a front of Fe^{3+} reduction within the quenched melt was observed and was identified as a diffusion-limited process. The growth of the reduced layer is accompanied by an increase in concentration of OH-groups suggesting that reduction operates through proton incorporation within the melt. As this growth rate is slightly faster than predicted from the diffusion of molecular H_2O, a different and mobile water-derived species seems likely. One possible mechanism is the reduction of Fe^{3+} by the transport of molecular H_2. As this process is limited by the flux of H_2, it will depend on both diffusivity and solubility of H_2 in the melt. Alternatively, migration of protons (H^+) and electronic species within the melt could control the velocity of the reduction front. The increase in concentration of the reaction-derived OH groups produces a water over saturation followed by partial dehydration of the melt. This dehydration leads to a change in the redox conditions within the gas that influences the Na partitioning between gas and melt.

INTRODUCTION

In concentrations ranging from parts per million to weight percent, hydrogen is always present in natural minerals or melts in the form of a variety of species with different redox states (H^+, OH^-, H_2O, or H_2) (Ingrin and Skogby 2000; Johnson et al. 1994; Schmidt et al. 1998; Stolper 1982). The identification of the nature and the mobility of the different H species is a key for understanding the Earth because H incorporation in mineral or melt dramatically modifies their physical properties. In nominally anhydrous minerals (NAM), the kinetics and mechanisms of H incorporation or extraction have been and still are studied intensively. Water-derived species incorporation/extraction in NAM recently has been revealed to evolve through a two-stage process (Kohlstedt and Mackwell 1998). The fastest stage was demonstrated to be related to redox processes involving H motion as protons and electronic defects related to Fe^{3+}-Fe^{2+} exchange (Kohlstedt and Mackwell 1998; Hercule and Ingrin 1999). Therefore, both the H content and Fe^{3+}/Fe^{2+} ratio in NAM are strongly interdependent parameters. The slower stage does not involve redox exchanges and seems to be associated with intrinsic defect mobility (Kohlstedt and Mackwell 1998).

With respect to silicate melts, it is generally accepted that H-bearing species diffuse as H_2O molecules (e.g., Zhang et al. 1991; Behrens and Nowak 1997). However, at low water contents (<0.8 wt%) the mobile water-derived species may be NaH_2O^+, H_3O^+, or H^+ (Stanton et al. 1990). Schmidt et al. (1998) have also identified the possibility of hydrogen incorporation as H_2 molecules in Fe-free silicate melts. In natural melts, which all contain H and Fe, redox interactions occur between H_2-H_2O and Fe^{3+}-Fe^{2+} (Gaillard et al. 2002). Currently, the mechanisms and the mobilities of the species involved in these interactions are still not known accurately.

Gaillard et al. (2002) studied the kinetics of Fe redox reactions at 2 kb in H_2O-rich (5–6 wt%), Fe-poor (1–3 wt% FeO_{tot}) melts that occur in response to variations of hydrogen fugacity (f_{H_2}). No redox fronts were observed. The kinetic data were interpreted in terms of a two-step reaction mechanism that involves first a virtually instantaneous diffusion of H_2 in the sample and then slower structural/chemical reorganizations, involving slower interactions of water-derived species with Fe in the melt. Oxidation-reduction of Fe in these low-Fe, high-H_2O rhyolitic melts is reaction-limited, in contrast to the diffusion-limited process identified by Cooper et al. (1996) for the oxidation of dry basaltic melts.

From these two studies, it is clear that the redox mechanisms in silicate melts strongly depend on the presence or absence of hydrogen (as H_2 and OH/H_2O). In addition, another major difference concerns the Fe concentration of the studied melts. Both factors make direct comparisons between the two studies difficult.

* Present address: Bayerisches Geoinstitut, Universität Bayreuth, D-95440 Bayreuth, Germany. E-mail: fabrice.galliard@uni-bayreuth.de

In this work, reduction experiments have been performed in a near-pure H_2 atmosphere on a nearly anhydrous Fe-rich silicate melt at low pressures to help elucidate the role of H_2 on redox mechanisms in the low-water concentration range. We show that, in contrast to previous observations for Fe-poor and high-H_2O melts, a redox front is clearly identified. We characterize the rate law for the progression of this redox front and the associated chemical mass transfers in the melt. We demonstrate that the process that rate-limits reduction is much slower than rates of molecular H_2 diffusion in the Fe-free system, but is slightly faster than molecular H_2O diffusion. Therefore, this study brings evidence that different water-derived species with different apparent mobilities may exist in silicate melts.

EXPERIMENTAL TECHNIQUES

Starting glass

Crystal-free, natural peralkaline obsidian was used as a starting material (Eburru, Kenya; MacDonald and Bailey 1973). The composition of the glass, including Fe and Fe_2O_3 (25% of iron as Fe^{3+}) and water content (0.25 wt% H_2O), is provided in Table 1. A series of 11 water content determinations, performed by FTIR (see Analyses), on different wafers yielded 0.25 ± 0.01 wt% H_2O, suggesting a homogeneous distribution of water-derived species in the starting glass.

The strong peralkalinity of this obsidian places the glass transition temperature at 400–500 °C, and allows us to perform low-temperature experiments under nearly dry conditions in the melt stability field without crystallization. A dry glass of the albite-orthoclase-quartz (AOQ) system was also used in one experiment as an Fe-free reference (Table 1).

Materials and strategy

Cylinders of the Eburru glass were placed in tubes of pure gold (ID = 5 mm, OD = 5.4 mm; the glass cylinder was cored using a drill of 5 mm ID). These assemblies, with one end of the capsule arc-welded and the other end open, were placed in cold-seal pressure vessels at 800 °C under 50 bars of pure H_2 for various durations (see Table 2). One additional experiment was performed using a platinum-capsule with one end sealed by an AOQ glass cap and the other end open to H_2 (Fig. 1a). The AOQ glass cap was formed by melting glass powder in the platinum-capsule at 1400 °C and 1 bar for 6 hours. A cylinder of Eburru glass was then placed in the same capsule in contact with the AOQ glass. This assembly was heated to 1200 °C at 1 bar for 7 minutes to make an airtight contact between the two glasses and between the samples and the capsule wall. The end of the capsule with the AOQ glass was cut so that the AOQ glass was directly exposed to the H_2 gas in the experiment, and thus behaved as a screen between one end of the Eburru glass and the H_2 atmosphere. The other end of the Eburru glass was in direct contact with H_2.

The vessels used in the experiments allow rapid heating and quenching to be performed by mechanically moving the sample rapidly while at pressure between the cool and hot parts of the vessel. Once the experimental temperature was attained (~30 min), the samples were moved to the hot part of the vessel. Using this strategy, each sample was heated from ambient temperatures to 800 °C within less than 5 min. After the experiment, the sample was quenched rapidly by moving it to the cool part of the vessel. Subsequently, the samples assemblies were cut into slices and polished for optical observation, electron microprobe analysis (EMPA), and infrared spectroscopy (FTIR). Wet-chemical analyses and Mössbauer spectroscopy were also performed on selected samples.

Analyses

EMPA was performed using an SX-50 Cameca electron microprobe under the following conditions: 15 kV accelerating potential, 6 nA beam current, 10–20 µm beam size, 10 s counting time on element peak positions and 5 s counting time on the background. Multi-element chemical profiles were performed with a 20 µm step increment across the sample.

FTIR analysis was performed on doubly polished samples using a Nicolet 760 Magna spectrometer equipped with an infrared microscope. A CaF_2 beamsplitter was used with a visible light source and liquid N_2 cooled MCT/A detector. The mean beam size was 80–100 µm. Total H_2O content was estimated from the height of the 3600 cm^{-1} stretching O-H band. The extinction coefficient of the 3600 cm^{-1} absorption band was calibrated against measurements using Karl-Fisher titration performed on the starting glass (Table 1). The extinction coefficient was determined to be 40 L/g/cm.

Wet-chemical techniques were used to determine the FeO content of selected samples. The method and its precision are detailed in Gaillard et al. (2001). Fe_2O_3 contents were obtained by subtraction of FeO from total Fe analyzed by EMPA. As wet chemistry is a bulk technique, only the samples interpreted as chemically homogeneous based on their uniform color were analyzed (samples Eb/0, Eb/6). In addition, analyses using the Mössbauer milliprobe (McCammon et al. 1991; McCammon 1994) were performed on sample no. Eb/5 with a spot size of ~300 µm to determine Fe^{3+}/Fe^{tot} in the two regions of the sample with different colors.

RESULTS

Optical observation

The glasses quenched from all time-series experiments showed a sharp contrast in color, having translucent-green rims and inner regions with the same dark color as the starting glasses (see Fig. 2). The boundary between translucent-green and dark

TABLE 1. EMP analyses of the starting Eburru Obsidian and the AOQ glass

Sample	SiO_2	TiO_2	Al_2O_3	MgO	FeO_{tot}	MnO	NiO	CaO	Na_2O	K_2O	SO_3	P_2O_5	Total
Eburru	70.13	0.28	8.16	0.02	6.84	0.23	0.04	0.21	6.48	4.40	0.01	0.02	96.81
Eburru	FeO = 5.31wt%, Fe_2O_3 = 1.7 wt%, H_2O = 0.25 wt%												
AOQ	70.10	0	12.10	0	0.02	0	0	0.03	4.40	5.10	0	0	98.75

Notes: Wet chemistry was used for FeO and Fe_2O_3 contents and H_2O was determined by Karl Fisher titration. All data are given in wt%.

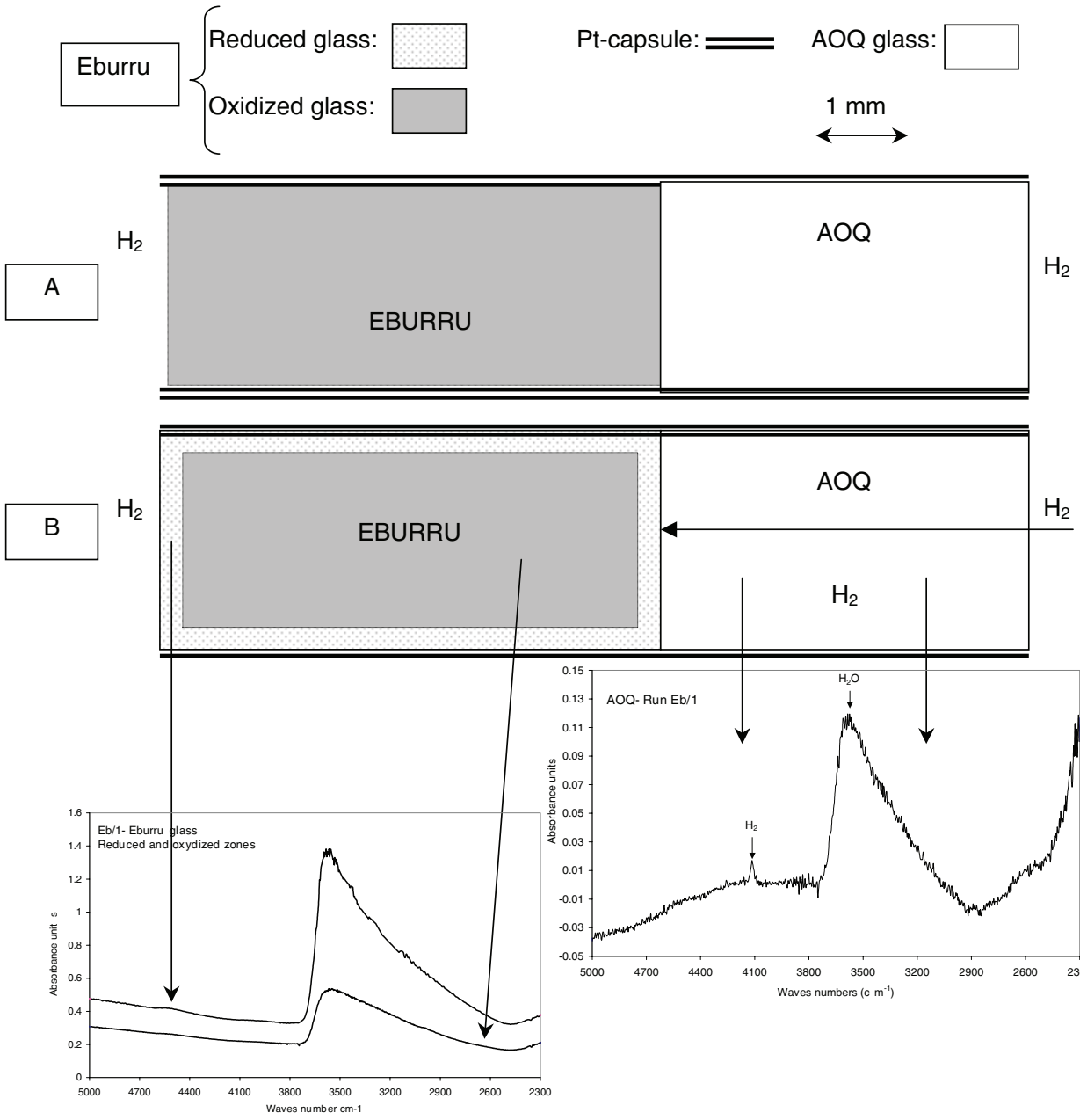

FIGURE 1. Sketch of the albite-orthoclase-quartz + Eburru glasses + Pt-capsule assembly used for experiments no. Eb/1. (**A**) Before experiments, (**B**) After experiments. FTIR spectra of AOQ (note the observed H_2-band) and both reduced and non-reacted zone of the Eburru glass are also shown. See text for additional details.

zones moved toward the inner part of the sample as the experiment duration increased. The rate of progression of this boundary was characterized optically. Table 2 summarizes the 6 observations from the 6 different run durations. After a run of 2916 min (~49 h), the sample was completely translucent-green (Eb/6). Micro-crystals were observed within the glasses after the runs. Using optical techniques we identified feldspar crystals, but these were not analyzed with the EMP.

Fe^{3+}/Fe^{tot}

Wet chemistry results, expressed in terms of Fe^{3+}/Fe^{tot}, are presented in Table 2. The starting obsidian (Eb/0) has $Fe^{3+}/Fe^{tot} = 0.23 \pm 0.05$, whereas sample no. Eb/6 was characterized as an essentially Fe^{3+}-free glass ($Fe^{3+}/Fe^{tot} = 0.01 \pm 0.01$). The two micro-Mössbauer analyses were performed on sample no. Eb/5 at the positions shown in Figure 2. The dark zone yielded $Fe^{3+}/Fe^{tot} = 0.25 \pm 0.05$, similar to the starting obsidian (Eb/0),

TABLE 2. Summary of the run conditions and descriptions of starting and run products

Sample name	Eb/0*	Eb/1	Eb/2	Eb/3	Eb/4	Eb/5	Eb/6
			Experimental: 800°C, f_{H_2} = 50 bar				
Run duration (Minutes)	0	30	65	90	150	180	2916
Capsule	–	Pt+AOQ	Au	Au	Au	Au	Au
				Optical			
Advancement of the reduction front in μm	0	180	302	355	430	480	>1800
			Fe^{3+}/Fe_{tot} (Wet chemical analyzes no. Eb/0 and Eb/6; Mössbauer analyzes no. Eb/5, see figure 2)				
Green zone	none	n.a	n.a	n.a	n.a	0	0
Dark zone	0.23	n.a	n.a	n.a	n.a	0.25	none
				FTIR (H_2O wt%)			
Green zone							
External†	none	0.66	n.a	0.57	0.41	0.43	0.42‡
Middle†	none		n.a	n.a	0.69	0.67	0.42‡
Internal†	none	0.75	0.74	0.73	0.71	0.73	0.42‡
Dark zone (homogeneous)	0.25	0.23	0.24	n.a	0.26	0.25	none

Notes: n.a. = Non analyzed; None = Not visible within the sample.
* Starting glass.
† Position relative to the sample geometry (see figure 2 for the location).
‡ 6 FTIR points were measured on this sample indicating a homogeneous H_2O content (±0.04 wt%).

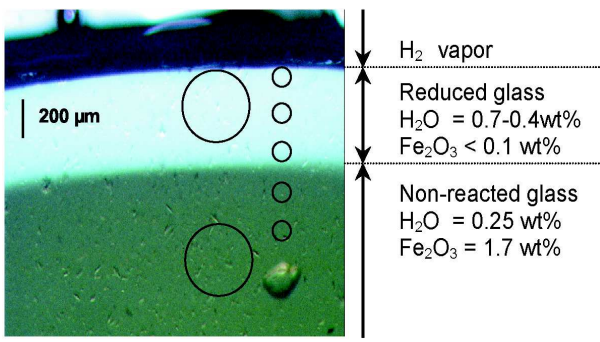

FIGURE 2. Transmitted light photomicrograph showing the change in color of the glass associated with reduction of Fe^{3+}. The two large circles indicate the location of the Mössbauer milliprobe analyses listed in Table 2. The five small circles illustrate the location of FTIR analyses from Table 2. Charge no. Eb/5.

whereas no Fe^{3+} was measurable in the green zone (Table 2). This observation gives credence to the argument that the difference of color between the green and dark zone indicates a strong difference of Fe redox state. Given the strongly reducing conditions of the experiment and the homogeneity of color within the green zone, we propose that the Fe^{3+} content is constant in this region and nearly equal to 0 for all runs (Table 2).

Major elements

EMP chemical profiles were performed on each experimental charge. In the run products no. Eb/1, no. Eb/2, and no. Eb/3, no clear major-element concentration variations were observed across the glasses. Comparisons with the starting glass revealed that Na content decreased by about 7% for all of these run products (Table 2). For samples no. Eb/4 and no. Eb/5, gradients in the concentration of Na at the samples rims were observed (Fig. 3). The maximum in Na concentration located at the gas-melt interface was equal to the Na content of the starting glass. Surprisingly, the position of this chemical gradient does not match that of the redox boundary. Rather, it is located behind the reduction front. Thus, for run no. Eb/5 (Figs. 2 and 3), the reduction front is at 480 μm from the sample surface, whereas the first evidence of Na motion was identified at 150–180 μm. No motion of other major elements was detected by EMPA (Fig. 3). For sample no. Eb/6, the Na_2O distribution within the sample was homogeneous and matched that of the starting glass.

H_2O

FTIR profiles were performed for several samples (see Table 2, and Figs. 2 and 3). In all samples analyzed, we observed water to be present mainly in the form of OH groups due to the dominance of the 4500 cm^{-1} O-H band over the 5200 cm^{-1} H_2O band. The green zone has significantly higher water contents than the dark zone (0.73–0.43 vs. 0.25 wt% H_2O, respectively). In the dark zone, the water content was similar to that of the starting glass. Between the green and the dark zones, the water content seems to decrease sharply although the spatial resolution of the FTIR analysis does not allow precise determination of the shape of the water profile at this boundary. The H_2O content of the green zone is not homogeneous. Rather, a maximum H_2O concentration is reached near the green/dark boundary (0.73 wt%) and it drops to ~0.43 wt% at the sample rims. For the longest experiment, no. Eb/6, the color and the chemical composition including H_2O content are homogeneous. The uniform H_2O content of 0.42 wt% is similar to the values measured at the edges of the other samples (Table 2).

H_2 mobility in melts

Experiment no. Eb/1, where the sample adjoined the AOQ glass, was characterized by growth of reduced green layers that are similar in width on the sides directly exposed to H_2 and in contact with the AOQ glass (Fig. 1). FTIR spectra were col-

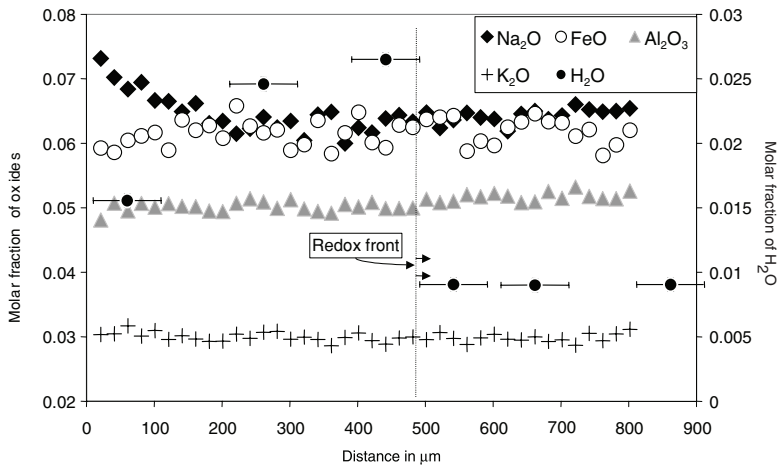

FIGURE 3. EMPA and FTIR profiles from sample no. Eb/5 (3 h). The zero value on the X-axis corresponds to the gas-melt interface. From this interface toward the sample interior, a strong Na decrease is observed. No clear variation of other elements can be identified except for water, shown as H_2O on the right axis. Note the difference in position of the redox front and the Na diffusion front. In 3 hours, molecular H_2O should have migrated over 220 µm (after Zhang et al. 1991), which correspond to the fronts of both Na migration and dehydration. The observed variations in Fe content are within the random variability observed across the whole profile.

lected on the AOQ sample before and after the experiment. The water content was about 0.01 wt% before and 0.015 wt% H_2O after the experiment (see Fig. 1). A striking peak at 4115 cm^{-1} was observed everywhere in the AOQ glass. This peak, which is always observed after annealing under very high f_{H_2} conditions (Schmidt et al. 1998), is due to molecular H_2 dissolved in the glass. This observation establishes unambiguously that, within a very short time, molecular H_2 had permeated the entire AOQ glass whose thickness is about 4 mm. No H_2 peak was observed for the Eburru glass in this experiment.

DISCUSSION

In these experiments, several reactions operate as suggested by the decoupling between H_2 mobility, Na migration and the reduction rate of Fe^{3+}. For clarity, hereafter we discuss separately the different processes.

Constraints on the $Fe^{3+} \rightarrow Fe^{2+}$ rate constant

Figure 4 shows a plot of the square of the reduction front position as a function of time. The linear relationship suggests that the reduction of Fe^{3+} to Fe^{2+} is a diffusion-limited process. The calculated slope gives the parabolic rate constant for $Fe^{3+} \rightarrow Fe^{2+}$ at 800 °C, $K_{Fe^{3+} \rightarrow Fe^{2+}} = 2 \times 10^{-11}$ m^2/s. Chekhmir et al. (1985) also observed the progression of a reduction front in albite melt (claimed to be $Mn^{7+} \rightarrow Mn^{2+}$), which they postulated to be controlled by diffusion and internal decomposition of molecular H_2. We calculated a parabolic rate constant from their single experiment and we find $K_{Mn^{7+} \rightarrow Mn^{2+}} = 2 \times 10^{-10}$ m^2/s at 1000 °C, which seems reasonably consistent with our lower temperature results. However, because Chekhmir et al. (1985) did not perform systematic time-series experiments, the comparison is tenuous. It is interesting to note that, in both studies, the parabolic rate constant is close to but slightly higher than the diffusion of molecular water [(~ 0.5 to 0.8 log unit higher, D_{H_2O} calculated after Zhang et al. (1991)]. For run no. Eb/5, the coupled incorporation of H plus the reduction of Fe^{3+} have progressed over 480 µm (Table 2), whereas in the same time, migration of molecular H_2O should have operated over ~220 µm. Thus, we have obtained evidence that redox interaction between H_2 and Fe gives rise to a transfer of water-derived species with mobilities different from molecular H_2O diffusion.

Constraints on H_2 mobility from no. Eb/1

The presence of molecular H_2 in the AOQ glass, and the similarity between the widths of the reduction rim at the H_2-melt and melt-AOQ interfaces, suggest that H_2 has diffused very rapidly through the AOQ melt (run no. Eb/1). We excluded the possibilities of H_2 migration at the AOQ-Eburru boundary because we consider the interface to be welded tightly in the previous anneal. We estimate that if H_2 had taken more than 5 min to cross the 4 mm length of the AOQ cap, we should have been able to see asymmetry in the width of the reduction rim. Therefore, we can calculate a minimum diffusion coefficient for molecular H_2 in the AOQ melt using the relationship $x = (D \cdot t)^{1/2}$, where x is the diffusion length (4 mm), D the diffusion coefficient, and t the minimum duration required for diffusion across the cap. We estimate $D_{H_2} \geq 10^{-8}$ m^2/s at 800 °C. This value is significantly higher than the diffusion coefficient proposed by Chekhmir et al. (1985) for diffusion of molecular H_2 in amorphous albite under essentially the same conditions.

Mechanisms of reduction: Ionic vs. molecular migrations

Macroscopically, reduction of a melt results from an increase of the cation/oxygen ratio. This can be accomplished by a loss of oxygen anions or by incorporation of cations (see Fig. 5 for an illustration of all the likely scenarios). The growth of reduced rim is accompanied by an abrupt increase of the OH content, which is consistent with an incorporation of protons (increase of cation/oxygen ratio). Mechanism 1, shown in Figure 5, involves inward migration of cations as a mirror image of the oxidation-reaction path operating under dry conditions (Cooper et al. 1996). As no migration of divalent cations was observed, this mechanism does not operate here.

From a microscopic point of view, there are several ways to incorporate these protons into the Eburru melt. If molecular hydrogen (H_2) solubility in the melt is sufficiently high, proton incorporation can be achieved by H_2 dissolution at the vapor-melt boundary together with H_2 diffusion within the melt plus H_2 breakdown by reduction of Fe^{3+} at the reduction front, resulting in the formation of two Fe^{2+} and two protons (see Fig. 5). In a peralkaline melt such as Eburru, Fe^{3+} (in tetrahedral coordination) is charge-compensated structurally by alkalis (Dickenson and Hess 1986). Therefore, to account for the in-

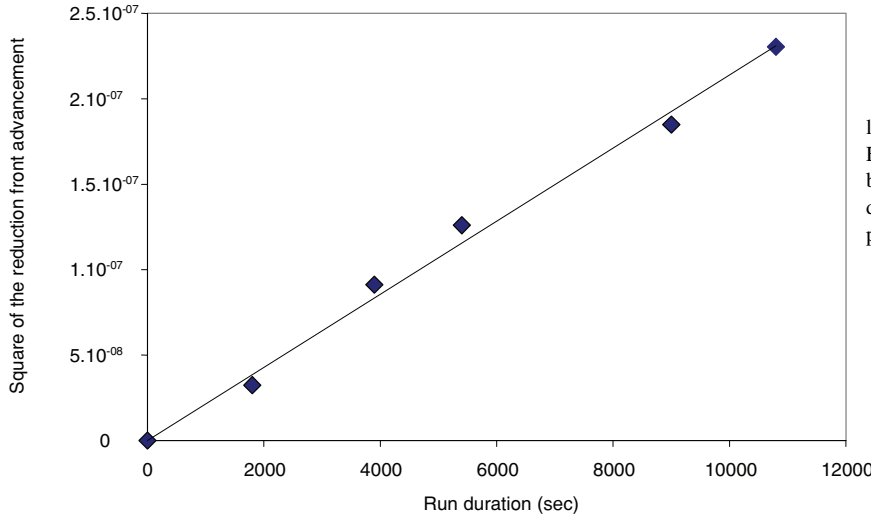

FIGURE 4. Identification of the kinetic law of Fe^{3+} reduction by hydrogen in the Eburru melt. The linear relationship between the square of the position and run duration indicates a diffusion-limited process.

crease of OH content accompanying reduction of Fe^{3+} by H_2, we write [in the notation of Hess (1980)]:

$$H_2 + 2\ NaFe^{3+}O_2 + 2\ SiOSi \rightarrow 2\ NaOH + 4\ (Fe^{2+})_{0.5}OSi \quad (1)$$

accompanied by a structural partioning of water:

$$NaOH + SiOSi \leftrightarrow NaOSi + HOSi. \quad (2)$$

If the rate of reduction is controlled by solubilization of molecular H_2 at the vapor-melt interface, the growth of the reacted layer should depend linearly on time. However, as the process shows a parabolic dependence on time, diffusion within the melt must be rate limiting. Diffusion of molecular H_2 in AOQ is 3 to 4 orders of magnitude faster than the growth rate of the reduction rim in Eburru. Either: (1) H_2 diffusion in the AOQ and Eburru melts are very different; (2) H_2 diffusion is rate-limiting, but additional processes delay the reduction rate of the Eburru melt; or (3) H_2 is not directly involved in the reaction and diffusion of H_2 is not rate limiting.

In the first case, no specific investigation on the compositional dependence of D_{H_2} is available. Hence, we cannot argue in favor of variable diffusion rates for hydrogen. However, many studies devoted to diffusion properties of neutral molecules in silicate melts [He, Ne, Ar, H_2O… see Watson (1994)] showed that the smaller the molecule is, the weaker is the compositional dependence of the diffusion coefficient. For He whose size is close to that of H_2, D_{He} varies by much less than one log unit between basalt and rhyolite (Watson 1994) whereas we observed a difference of 3 log unit between D_{H_2} in AOQ and the reaction rate in Eburru. We therefore consider that even if D_{H_2} can be different in the AOQ and Eburru melts, this difference cannot explain the contrast in velocity between D_{H_2} in AOQ and the reaction rate in Eburru.

For the second case (Fig. 5, mechanism 2), Crank (1975) gave an approximate solution for the growth of the reaction layer controlled by the dissolution rate of a reactive gas.

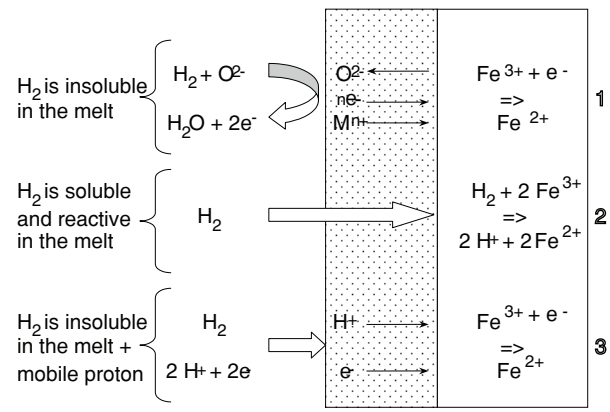

FIGURE 5. Flow chart illustrating the different likely mechanisms for Fe^{3+} reduction in the Eburru melt. All of these mechanisms must satisfy a required increase of the cation/anion ratio: (**1**) Molecular H_2 is not soluble in the melt, therefore reduction proceeds through O extraction, which is rate-limited by inward migrations of cations or electronic species; this scenario is the mirror image of the oxidation mechanisms observed by Cooper et al. (1996). (**2**) Adsorption, diffusion, and reaction of molecular H_2 with Fe^{3+} in the melt. (**3**) Molecular H_2 is not soluble in the melt but inward migration of protons and electronic species may occur producing the reduction.

$$X = [(2D_{H_2} \cdot S_{H_2} \cdot t)/(2\ C_{Fe^{3+}})]^{1/2} \quad (3)$$

where D, S, and C are, respectively, the diffusion coefficient, solubility, and concentration of the subscripted species, and X gives the thickness of the reacted layer as a function of time, t. This equation may provide an explanation for the difference between the reaction rate and the diffusivity of the mobile species. In the present case, if the ratio $S_{H_2}/2\ C_{Fe^{3+}} \ll 1$ but still large enough that transport of molecular H_2 dominates the reduction process, the growth of the reduced rim can be much slower than diffusion of H_2 while still obeying a diffusion-lim-

ited law. The lack of an H_2 signature in the infrared spectra of the Eburru glass is consistent with this solubility criterion.

In the third case, if we consider that molecular H_2 is so insoluble in the melt that there are insufficient H_2 species available to reduce the Fe^{3+}, other water-derived species must be rate limiting. Thus, molecular H_2 may react with Fe^{3+} to produce Fe^{2+} and OH groups at the gas-melt interface, as shown in Equation 1. Then the redox potential is conveyed toward the interior of the sample by coupled transport of protons and electronic species (see Fig. 5, mechanism 3). In Equation 1, H_2 should then be replaced by H^+ and electrons e^- or electron holes h^+. Because Fe-bearing glasses and melts are polaron-type semiconductors (Cooper et al. 1996, and references therein), such migration of cations in a redox gradient is charge-compensated by electronic migration. Diopside (Hercule and Ingrin 1999) and olivine crystals (Kohlstedt and Mackwell 1998) have been shown to facilitate incorporation of protons coupled to outward migration of electron holes caused by reduction of Fe^{3+}. In that case, the growth rate of the reduced rim is controlled either by proton or electronic mobilities. According to Schmalzried (1981), the width of the reacting layer is directly proportional to the square root of time, t, to the diffusion coefficient of the rate-limiting species i (H^+ or electronic species), and to the Gibbs free energy of the ongoing reaction normalized by the temperature, T:

$$X = [\ 2\ D_i \cdot \Delta G\ /\ (RT) \cdot t\ ]^{1/2} \quad (4)$$

In general, proton diffusion in SiO_2-rich silicate melts is not regarded as a likely mechanism (Zhang et al. 1991; Nowak and Behrens 1997). Although Behrens and Nowak (1997) ruled out the possibility of proton migration in Fe-free SiO_2-rich melt, incorporation of Fe may introduce electron holes (Fe^{3+}) that provide charge compensation for proton jumps. Also, according to Stanton et al. (1990) (see also the review of Dingwell 1995), a mobile, positively charged H-bearing species can dominate the transport of water-derived species in low-H_2O melts (<0.8 wt% H_2O; Stanton et al. 1990). This mobile, water-derived species could be NaH_2O^+, H_3O^+, or H^+. We can exclude NaH_2O^+ in our experiments because the chemical profile for Na does not extend all the way to the redox front. A mass-balance calculation, based on the Mössbauer data (Fe^{3+}/Fe_{tot}) and FTIR spectra (OH) close to the reduction front, indicates variation of Fe^{3+} and OH concentration that reasonably matches with proton rather than H_3O^+ incorporation (one OH band created for the reduction of one Fe^{3+}). Therefore, the parabolic rate constant extracted from Figure 4 should reflect either proton or electron migration rates, depending on which is the slowest.

Na migration

The migration of Na seems to be decoupled kinetically from the redox interaction between H_2 and iron. A rapid decrease in the Na content (of ~7%) is observed within the first 30 min of exposure to an H_2 gas. We interpret these results as the consequence of the redox partitioning of Na between melt and gas already observed under H-free conditions (see Georges et al. 2000). The f_{O_2} during the beginning of the runs is very reducing so that it causes a displacement toward the RHS of the following equilibria:

$$Na_2O^{melt} \leftrightarrow Na_2^{gas} + {}^1/_2O_2^{gas} \quad (5)$$

As we did not observe any Na gradient in sample no. Eb/1, the above equilibria should be achieved very rapidly consistent with very high Na diffusion rate in peralkaline melts (Henderson et al. 1985). Molecular O_2^{gas} is not stable, as H_2O will be produced instead at the melt/gas interface by oxidation of H_2 by Na_2O. This oxidation may effect a small, transient change in the f_{O_2} of the gas near the surface of the melt. In sample no. Eb/4 and no. Eb/5 (Fig. 3), as well as dehydration of the melt, we observed chemical migration of Na. The release of water into the gas phase should increase the f_{H_2O}/f_{H_2} ratio and therefore increase the f_{O_2} in the gas. Equation 5 is therefore displaced to its LHS and Na migration from the gas toward the melt occurs. Figure 3 shows that the position of both Na migration and dehydration fronts nearly corresponds to the calculated position of a front of molecular H_2O migration [calculated after Zhang et al. (1991), see caption of Fig. 3]. Therefore, we anticipate that migration of Na from the gas to the melt operated at a rate controlled by melt dehydration (i.e., H_2O mobility) and not by Na diffusion in the melt.

Comparison with previous work

The kinetics of Fe oxidation-reduction in anhydrous basaltic melts has been demonstrated to be rate-limited by diffusion of divalent cations (Cooper et al. 1996; Cook and Cooper 2000). In contrast, we provide clear evidence that, for low H_2O melts, molecular hydrogen or coupled proton-electronic species are the mobile species controlling the advance of the reduction front. The kinetics of change in Fe^{3+}/Fe^{2+} is thus much faster in H-bearing systems than in anhydrous systems (representing the several orders of magnitude difference between Ca^{2+} and H_2, H^+ diffusion rates). Given that H-bearing species are always present in natural magmas, modification of the Fe redox state is most likely to occur following the mechanisms we have identified in this study. It should be noted, however, that for high-H_2O, low-Fe melts, Gaillard et al. (2002) have not detected any coupled proton/electronic species motion. The reason for this discrepancy may be due to reduced electronic conductivity in Fe-poor melts and/or high concentration of water in the melts that may affect both diffusion and solubility of H_2.

Concluding remarks and perspectives

The major points from this study are: (1) reduction of Fe^{3+} in the melt by H_2 operates by the progression of a redox front that is accompanied by an increase in the concentration of OH-groups; (2) H_2 diffusion in silicate melts is much more rapid than the observed rate of reduction of Fe^{3+}; (3) the velocity of the redox front within the melt is faster than the mobility of molecular H_2O, suggesting that various hydrogen-bearing species with different diffusivities may exist in a silicate melt; and (4) exchange of Na between the gas and the melt occur at a very high rate and are extremely sensitive to the redox conditions.

Understanding the response of a magma to changes in its environment, such as during degassing or exchanges during mixing or interaction with surrounding solids requires the

knowledge of the identity and the mobility of all H-derived species. In this study, we have shown that redox exchanges between H and Fe causes incorporation of OH groups at a rate different from H_2O migration. We have also shown that the H content and Fe^{3+}/Fe^{2+} ratios in melt are strongly correlated. We should thus question the robustness of Fe^{3+}/Fe^{2+} of melts as an indicator of pre-eruptive oxygen fugacity because these melts may have undergone degassing (Christie et al. 1986). Further studies, however, are clearly needed to quantify the relationship between Fe redox state and H incorporation/extraction for a range of melts compositions and experimental conditions that permit direct comparison with natural magma processes.

ACKNOWLEDGMENTS

Interpretations of the experimental data were greatly enhanced by discussions with Reid Cooper and Rebecca Everman. Julian Mecklenburgh made a useful informal review of the final version. Ray MacDonald, who kindly supplied the Eburru glass, is also thanked. Hans Keppler and Max Wilke are acknowledged for their reviews. Mike Toplis is greatly thanked for the editorial work.

REFERENCES CITED

Behrens, H. and Nowak, M. (1997) An experimental investigation on diffusion of water in haplogranitic melts. Contribution to Mineralogy and Petrology, 126, 365–376.

Chekhmir, A.S, Persikov, E.S., Epel´Baum, M.B., and Bukhtiyarov, P.G. (1985) Experimental investigation of the hydrogen transport through the model magmatic melt. Geokhimya, 5, 594–598.

Christie, D.M., Carmichael, I.S.E., and Langmuir, C.H. (1986) Oxidation state of mid-ocean ridge basalt glasses. Earth Planetary Science Letters, 79, 397–411.

Cook, G.B. and Cooper, R.F. (2000) Iron concentration and the physical processes of dynamic oxidation in alkaline earth aluminosilicate glass. American Mineralogist, 85, 397–406.

Cooper, R.F, Fanselow, J.B, and Poker, D.B (1996) The mechanism of oxidation of a basaltic glass: Chemical diffusion of network-modifying cations. Geochimica et Cosmochimica Acta, 60, 3253–3265.

Crank, J. (1975) Mathematics of diffusion. Oxford University Press, U.K.

Dickenson, M.P. and Hess, P.C. (1986) The structural role and homogeneous redox equilibria of iron in peraluminous, metaluminous and peralkaline silicate melts. Contributions to Mineralogy and Petrology, 92, 207–217.

Dingwell, D.B. (1995) Relaxation theory in silicate melts. In J. Stebbins, P.F. McMillan and D.B. Dingwell, Eds., Structure, Dynamics and Properties of Silicate Melts, 32, 23–48. Reviews in Mineralogy, Mineralogical Society of America, Washington, D.C.

Gaillard, F., Scaillet, B., Pichavant, M., and Beny, J.M. (2001) The effect of water and f_{O_2} on the ferric-ferrous ratio of silicic melts. Chemical Geology, 174, 255–273.

Gaillard, F., Scaillet, B., and Pichavant, M. (2002) Kinetics of iron oxidation-reduction in hydrous silicic melts. American Mineralogist, 87, 829–837.

Georges P., Libourel G., and Deloule E. (2000) Experimental constraints on alkali condensation in chondrule formation. Meteorites and Planetary Sciences, 35, 1183–1186.

Henderson, P., Nolan, J., Cunningham, G.C., and Lowry, R.K. (1985) Structural controls and mechanisms of diffusion in natural silicate melts. Contribution to Mineralogy and Petrology, 89, 263–272.

Hercule, S. and Ingrin, J. (1999) Hydrogen in diopside: Diffusion, kinetics of extraction-incorporation, and solubility. American Mineralogist, 84, 1577–1587.

Hess, P.C. (1980) Polarization model for silicate melts. In R.B. Hargraves, Ed., Physics of magmatic processes, 3–48. Princeton University Press, New Jersey.

Ingrin, J. and Skogby, H. (2000) Hydrogen in nominally anhydrous upper-mantle minerals: concentration levels and implications. European Journal of Mineralogy, 12, 543–570.

Johnson, M.C., Anderson, A.T., and Rutherford, M.J. (1994) Pre-eruptive volatile contents of magmas. In M.R. Carroll and John R. Holloway, Eds., Volatiles in magmas, 30, 281–323. Reviews in Mineralogy, Mineralogical Society of America, Washington, D.C.

Kohlstedt, D.L and Mackwell, S.J. (1998) Diffusion of hydrogen and intrinsic point defects in olivine. Zeitschrift für physikalische Chemie, 207, 147–162.

Macdonald, R. and Bailey, D.K. (1973). The chemistry of the peralkaline oversaturated obsidians. U.S. Geological Survey Professional Papers 440-N, Part 1, 1–37.

McCammon, C. (1994) A Mössbauer milliprobe: Practical considerations. Hyperfine Interactions, 92, 1235–1239.

McCammon, C.A., Chaskar, V., and Richards, G.G. (1991) A technique for spatially resolved Mössbauer spectroscopy applied to quenched metallurgical slags. Measurement Science Technology, 2, 657–662.

Nowak, M. and Behrens, H. (1997) The mechanisms of water diffusion in polymerized silicate melts. Contribution to mineralogy and petrology, 126, 377–385.

Schmalzried, H. (1981) Solid state reaction, Verlag Chemie, Weinheim.

Schmidt, B.C., Holtz, F.M., and Beny, J-M. (1998) Incorporation of H_2 in vitreous silica, qualitative and quantitative determination from Raman and infrared spectroscopy. Journal of Noncrystalline Solids, 240, 91–103.

Stanton, T.R., Tyburczy, J.A., Holloway, J.R., and Petuskey, W.T. (1990) Electromigration of water in silicate glass: Resolution of the valence charge of the diffusing species. EOS Transactions AGU, 71, 652.

Stolper, E. (1982) The speciation of water in silicate melts. Geochimica et Cosmochimica Acta, 46, 2606–2620.

Watson, E.B. (1994) Diffusion in volatile-bearing magmas. In M.R. Carroll and John R. Holloway, Eds.,Volatiles in magmas, 30, 371–411. Reviews in Mineralogy, Mineralogical Society of America, Washington, D.C.

Zhang, Y., Stolper, E.M., and Wasserburg, G.J. (1991) Diffusion of water in rhyolitic glasses. Geochimica Cosmochimica Acta, 55, 441–456.

MANUSCRIPT RECEIVED NOVEMBER 6, 2001
MANUSCRIPT ACCEPTED OCTOBER 8, 2002
MANUSCRIPT HANDLED BY MICHAEL TOPLIS